

Experimental bounds on collapse models from gravitational wave detectors

Matteo Carlesso,^{1,2,*} Angelo Bassi,^{1,2,†} Paolo Falferi,^{3,4} and Andrea Vinante³

¹*Department of Physics, University of Trieste, Strada Costiera 11, 34151 Trieste, Italy*

²*Istituto Nazionale di Fisica Nucleare, Trieste Section, Via Valerio 2, 34127 Trieste, Italy*

³*Istituto di Fotonica e Nanotecnologie, CNR - Fondazione Bruno Kessler, I-38123 Povo, Trento, Italy*

⁴*INFN - Trento Institute for Fundamental Physics and Applications, I-38123 Povo, Trento, Italy*

(Dated: March 21, 2022)

Wave function collapse models postulate a fundamental breakdown of the quantum superposition principle at the macroscale. Therefore, experimental tests of collapse models are also fundamental tests of quantum mechanics. Here, we compute the upper bounds on the collapse parameters, which can be inferred by the gravitational wave detectors AURIGA, LIGO and LISA Pathfinder. We consider the most widely used collapse model, the Continuous Spontaneous Localization (CSL) model. We show that these experiments exclude a huge portion of the CSL parameter space, the strongest bound being set by the recently launched space mission LISA Pathfinder.

1. INTRODUCTION

Wavefunction collapse models aim at solving the measurement problem of quantum mechanics, that is the apparent contradiction between the linear and deterministic evolution of quantum systems and the nonlinear stochastic collapse of the wavefunction during the measurement process [1–3]. The general assumption is that the quantum superposition principle breaks down at the macroscale due to a fundamental localization mechanism. In order to recover standard quantum mechanics at the microscale, the strength of the localization mechanism is assumed to be extremely weak at single particle level, while rapidly increasing with the number of constituents.

The most widely used collapse model is the so called Continuous Spontaneous Localization (CSL) model [4], which is based on two unknown constants, a characteristic length r_C , characterizing the spatial resolution of the stochastic collapse mechanism, and the collapse rate λ . The standard theoretical values commonly reported in literature are respectively $r_C = 10^{-7}$ m, $\lambda = 10^{-17}$ s⁻¹ following Ghirardi, Rimini and Weber (GRW) [1, 4] and $r_C = 10^{-7}$ m, $\lambda = 10^{-8\pm2}$ s⁻¹ or $r_C = 10^{-6}$ m, $\lambda = 10^{-6\pm2}$ s⁻¹ following Adler [5]. These values are obtained when imposing in a somehow arbitrary way that macroscopic (in GRW case) or mesoscopic (Adler) quantum superpositions will collapse in a reasonably short time. However, as the model is phenomenological, there is actually no fundamental way to predict the values of r_C and λ . At present, GRW values can be regarded as a sort of lower limit, in the sense that weaker value of λ would not guarantee a sufficiently rapid collapse of macroscopic human-scale quantum superpositions and this runs counter the original motivation of the model [6].

Experimental tests of the CSL model can be done either with matter-wave interference experiments [7–13] or with noninterferometric methods [14–21]. The strongest experimental upper bounds so far have been set by the latter, in particular by X-ray spontaneous emission for $r_C < 10^{-6}$ m [22] and by force noise measurements on ultracold cantilevers for $r_C > 10^{-6}$ m [23].

Here, we analyze the upper bounds that can be inferred by precision experiments based on macroscopic mechanical systems, focusing in particular on gravitational wave (GW) detectors. We will argue that GW detectors and related experiments, in particular the recently launched space mission LISA Pathfinder, set the strongest upper limits for $r_C > 10^{-6}$ m thereby excluding a huge portion of the CSL parameter scale. In section 2 we will outline the theoretical model, in section 3 we will derive the upper limit from three relevant experiments, respectively AURIGA [24], advanced LIGO [25] and LISA Pathfinder [26]. In section 4 we will discuss the upper limits and compare them with the other existing bounds.

2. THEORETICAL MODEL

The three experiments (AURIGA, LIGO and LISA Pathfinder) here considered represent the state of the art in their class, respectively resonant mass GW detectors, ground-based interferometric detectors, and precursors of space-born detectors. A GW detector monitors the deformation of space-time. The strain noise spectrum $S_{hh}(\omega)$ quantifies the strength of such a deformation.

AURIGA is based on a single cylindrical bar mechanical oscillator, while LIGO and LISA Pathfinder monitor the optical distance between pairs of nominally free masses (see Fig. 1). In the first case the CSL noise causes a driving

force on the bar oscillator; in the second case it acts on the relative distance between the two masses. We will consider both cases.

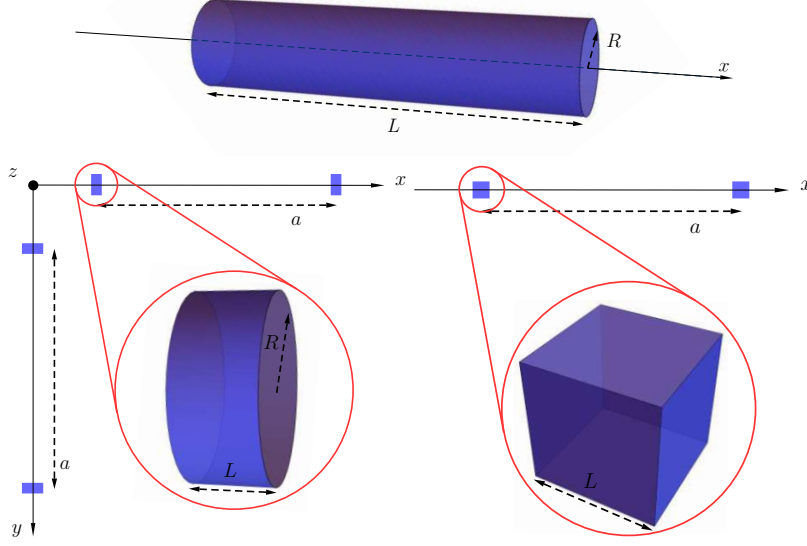


FIG. 1: Graphical representation of the three experiments here considered; the images are not in scale. AURIGA is on the top, LIGO on the bottom left and LISA Pathfinder on the bottom right. AURIGA features a cylindrical single mass (radius R , length L), aligned with respect to the direction x of measurement. In LIGO, four identical cylindrical masses (radius R and length L) are arranged as in Figure; a is the distance between the center-of-mass of two masses on a single arm of the interferometer. The arms are oriented along the x and y directions. LISA Pathfinder features two cubic (length L) masses, displaced along the x direction with relative distance between their center-of-mass equal to a .

The dynamics of the (mass proportional) CSL model is given by the following non-linear and stochastic differential equation [27]:

$$d|\psi_t\rangle = \left(-\frac{i}{\hbar} \hat{H} dt + \frac{\sqrt{\lambda}}{\pi^{3/4} m_0 r_C^{3/2}} \int d\mathbf{z} \left(\hat{M}(\mathbf{z}) - \langle \hat{M}(\mathbf{z}) \rangle_t \right) dW_t(\mathbf{z}) - \frac{\lambda}{2\pi^{3/2} m_0^2 r_C^3} \int d\mathbf{z} \left(\hat{M}(\mathbf{z}) - \langle \hat{M}(\mathbf{z}) \rangle_t \right)^2 dt \right) |\psi_t\rangle, \quad (1)$$

where m_0 is the reference mass chosen equal to the mass of a nucleon, and $\hat{M}(\mathbf{z})$ is defined as:

$$\hat{M}(\mathbf{z}) = m_0 \sum_n e^{-\frac{(\mathbf{z} - \hat{\mathbf{q}}_n)^2}{2r_C^2}}, \quad (2)$$

where the sum runs on the N nucleons of the system, which have position operator $\hat{\mathbf{q}}_n$, and $\{W_t(\mathbf{z})\}$ is an ensemble of Wiener processes uncorrelated in space. The term $\langle \hat{M}(\mathbf{z}) \rangle_t = \langle \psi_t | \hat{M}(\mathbf{z}) | \psi_t \rangle$ is responsible for the non-linearity of the evolution. The corresponding master equation for the density matrix $\hat{\rho}(t)$ is [2]:

$$\frac{d}{dt} \hat{\rho}(t) = -\frac{\lambda}{2r_C^3 \pi^{3/2} m_0^2} \int d\mathbf{z} \left[\hat{M}(\mathbf{z}), \left[\hat{M}(\mathbf{z}), \hat{\rho}(t) \right] \right], \quad (3)$$

Let us divide the total mass in a subset of masses, labeled by α : for AURIGA we have a single cylindrical mass ($\alpha = 1$), for LISA Pathfinder we have two mass distributions ($\alpha=1$ and 2), while for LIGO we have 4 mass distributions, but we will consider the two arms separately (so again $\alpha=1$ and 2). Then, the position operator $\hat{\mathbf{q}}_n$ can be written as follows [17, 18]:

$$\hat{\mathbf{q}}_n = \mathbf{q}_{n,\alpha}^{(0)} + \hat{\mathbf{q}}_\alpha + \Delta \hat{\mathbf{q}}_{n,\alpha}, \quad (4)$$

where $\mathbf{q}_{n,\alpha}^{(0)}$ is the classical rest position of the n -th particle (belonging to the α -th distribution), $\hat{\mathbf{q}}_\alpha$ measures the fluctuations of the α -th center-of-mass with respect to its classical rest position and $\Delta \hat{\mathbf{q}}_{n,\alpha}$ is the displacement of the n -th particle with respect to the α -th center-of-mass. Assuming the mass distributions are rigid, $\Delta \hat{\mathbf{q}}_{n,\alpha}$ can be

safely neglected. When the spread of the center-of-mass wave-function is much smaller than r_C , Eq. (2) can be Taylor expanded up to the first order of the fluctuations $\hat{\mathbf{q}}_\alpha$ and becomes:

$$\hat{M}(\mathbf{z}) \approx M_0(\mathbf{z}) + \sum_{\alpha} \int \frac{d\mathbf{x}}{r_C^2} \sigma_{\alpha}(\mathbf{x}) e^{-\frac{(\mathbf{z}-\mathbf{x})^2}{2r_C^2}} (\mathbf{z}-\mathbf{x}) \cdot \hat{\mathbf{q}}_{\alpha}, \quad (5)$$

where $M_0(\mathbf{z})$ is a \mathbb{C} -function, and $\sigma_{\alpha}(\mathbf{x}) = m_0 \sum_n \delta^{(3)}(\mathbf{x} - \mathbf{q}_{n,\alpha})$ is the α -th mass distribution. Here the sum runs on the nucleons belonging to the α -th mass. Eq. (3) becomes

$$\frac{d}{dt} \hat{\rho}(t) = -\frac{1}{2} \sum_{\alpha, \beta} \sum_{i, j=x, y, z} \eta_{ij}^{\alpha, \beta} [\hat{q}_{\alpha, i}, [\hat{q}_{\beta, j}, \hat{\rho}(t)]], \quad (6)$$

where $\hat{q}_{\alpha, i}$ is the i -th component of $\hat{\mathbf{q}}_{\alpha}$, and the diffusion CSL rate is given by

$$\eta_{ij}^{\alpha, \beta} = \frac{\lambda}{r_C^7 \pi^{3/2} m_0^2} \int d\mathbf{z} \int d\mathbf{x} \int d\mathbf{y} \sigma_{\alpha}(\mathbf{x}) \sigma_{\beta}(\mathbf{y}) e^{-\frac{(\mathbf{z}-\mathbf{x})^2}{2r_C^2}} e^{-\frac{(\mathbf{z}-\mathbf{y})^2}{2r_C^2}} (\mathbf{z}-\mathbf{x})_i (\mathbf{z}-\mathbf{y})_j. \quad (7)$$

Since we are interested only in the motion along the direction of detection, we can reduce the master equation (6) to its one-dimensional version, i.e. only the x -component is considered.

The dynamics of the master equation in Eq. (3) can be mimicked by a standard Schrödinger equation with an additional stochastic potential of the form

$$\hat{V}_{\text{CSL}}(t) = -\frac{\hbar\sqrt{\lambda}}{\pi^{3/4} r_C^{3/2} m_0} \int d\mathbf{z} \hat{M}(\mathbf{z}) w_t(\mathbf{z}), \quad (8)$$

where $w_t(\mathbf{z}) = dW_t(\mathbf{z})/dt$ is a white noise defined by $\langle w_t(\mathbf{z}) \rangle = 0$ and $\langle w_t(\mathbf{z}) w_s(\mathbf{y}) \rangle = \delta(t-s) \delta^{(3)}(\mathbf{z}-\mathbf{y})$. Such a stochastic potential acts on the α -th mass as a stochastic force, which in the same limit of validity of the expansion in Eq. (5), becomes

$$\mathbf{F}_{\alpha}(t) = \frac{\hbar\sqrt{\lambda}}{\pi^{3/4} r_C^{3/2} m_0} \int d\mathbf{z} \int \frac{d\mathbf{x}}{r_C^2} \sigma_{\alpha}(\mathbf{x}) e^{-\frac{(\mathbf{z}-\mathbf{x})^2}{2r_C^2}} (\mathbf{z}-\mathbf{x}) w_t(\mathbf{z}). \quad (9)$$

Notice that the noise $w_t(\mathbf{z})$ is spatially uncorrelated: it acts randomly and independently on every nucleon of the system. On the other hand, the smearing function defined in the operator in Eq. (2) introduces a spatial correlation, as we will see.

We now consider the x -direction of the motion of each mass of the system, modelled as the one of an harmonic oscillator of mass m_{α} and resonant frequency ω_{α} . The corresponding quantum Langevin equations read:

$$\frac{d}{dt} \hat{x}_{\alpha}(t) = \frac{\hat{p}_{\alpha}(t)}{m_{\alpha}} \quad \text{and} \quad \frac{d}{dt} \hat{p}_{\alpha}(t) = -m\omega_{\alpha}^2 \hat{x}_{\alpha}(t) - \gamma_{\alpha} \hat{p}_{\alpha}(t) + F_{\alpha}(t), \quad (10)$$

where $\hat{p}_{\alpha}(t)$ is the momentum of the α -th mass in x -direction. Here we have added as usual a dissipative term $-\gamma_{\alpha} \hat{p}_{\alpha}(t)$, which can be expressed in terms of the quality factor of the system $Q_{\alpha} = \omega_{\alpha}/\gamma_{\alpha}$, and $F_{\alpha}(t)$ is the x component of the stochastic force in Eq. (9). A more general treatment should include additional noise terms to take into account the action of the environment and the measurement apparatus. However, since we are primarily interested in estimating the effect of the CSL field, we neglect all other noise sources. Furthermore, the actual noise of the systems we will consider in the following is indeed the sum of several noise sources (e.g thermal, quantum, seismic, gravity gradient, etc.) but it is typically difficult to accurately distinguish and characterize each single contribution. This is particularly the case for interferometric detectors. In order to set an upper limit on CSL parameters we will take a conservative approach by assuming that all the experimentally measured noise is attributed to CSL. The physical quantity we are interested in is the force noise spectral density $S_{\text{FF}}(\omega) = \frac{1}{4\pi} \int_{-\infty}^{+\infty} \langle \{\tilde{F}(\omega), \tilde{F}(\Omega)\} \rangle$, expressed in $\text{N}^2 \text{Hz}^{-1}$, where $\tilde{F}(\omega)$ is the Fourier transform of the x component of stochastic force.

In the case of AURIGA, we have a single mass and the label α in Eq. (9) can be dropped. By using this expression and $\sigma(\mathbf{r})$ equal to that of the one of an homogeneous cylinder of radius R and length L , we obtain the following expression for the force noise spectral density

$$S_{\text{FF}}^{\text{AURIGA}}(\omega) = \frac{8\hbar^2\lambda}{L^2} \left(\frac{m}{m_0}\right)^2 \left(\frac{r_C}{R}\right)^2 \left(1 - e^{-\frac{L^2}{4r_C^2}}\right) \left[1 - e^{-\frac{R^2}{2r_C^2}} \left(\text{I}_0\left(\frac{R^2}{2r_C^2}\right) + \text{I}_1\left(\frac{R^2}{2r_C^2}\right)\right)\right], \quad (11)$$

where I_0 and I_1 denotes the first two modified Bessel functions of the first kind, and the correlations for the Fourier transformed white noise is $\langle \tilde{w}_\omega(\mathbf{z}) \tilde{w}_\Omega(\mathbf{y}) \rangle = 2\pi \delta(\omega + \Omega) \delta^{(3)}(\mathbf{z} - \mathbf{y})$. The force noise spectral density can be equivalently obtained by using $S_{\text{FF}}^{\text{AURIGA}}(\omega) = 2\hbar^2 \eta^{\text{AURIGA}}$, where the CSL diffusion rate η^{AURIGA} can be computed from Eq. (7) with $\alpha = \beta = 1$ and $i = j = x$.

In the case of LISA Pathfinder and the single arm of LIGO, there are two equal masses at an average distance a and the monitored motion is the relative one, which is described by the following Langevin equations:

$$\frac{d}{dt} \hat{x}_{\text{rel}}(t) = \frac{2\hat{p}_{\text{rel}}(t)}{m} \quad \text{and} \quad \frac{d}{dt} \hat{p}_{\text{rel}}(t) = -\frac{m}{2} \omega_0^2 \hat{x}_{\text{rel}}(t) - \gamma \hat{p}_{\text{rel}}(t) + F_{\text{rel}}(t), \quad (12)$$

where $F_{\text{rel}}(t) = \frac{1}{2}(F_1(t) - F_2(t))$. The corresponding force noise spectral density is given by

$$S_{\text{FF}}^{\text{L}}(\omega) = \frac{\hbar^2 \lambda r_C^3}{2\pi^{3/2} m_0^2} \int d\mathbf{k} |\tilde{\sigma}(\mathbf{k})|^2 (1 - e^{iak_x}) k_x^2 e^{-r_C^2 \mathbf{k}^2}. \quad (13)$$

Here, there are two CSL contributions to the motion: the incoherent action on the single mass (first term in parenthesis) and the correlation between the two masses (second term) which are relevant when $a < r_C$. By substituting $\sigma_\alpha(\mathbf{r})$ with the α -th mass distribution, a cylinder (radius R and length L) for LIGO and a cube (length L) for LISA Pathfinder, we obtain from Eq. (13) the following expressions:

$$\begin{aligned} S_{\text{FF}}^{\text{LIGO}}(\omega) &= \frac{8\hbar^2 \lambda}{L^2} \left(\frac{m}{m_0}\right)^2 \left(\frac{r_C}{R}\right)^2 \left[1 - e^{-\frac{R^2}{2r_C^2}} \left(I_0\left(\frac{R^2}{2r_C^2}\right) + I_1\left(\frac{R^2}{2r_C^2}\right) \right) \right] f_{\text{corr}}, \\ S_{\text{FF}}^{\text{LISA}}(\omega) &= \frac{16\hbar^2 \lambda}{L^2} \left(\frac{m}{m_0}\right)^2 \left(\frac{r_C}{L}\right)^4 \left(1 - e^{-\frac{L^2}{4r_C^2}} - \sqrt{\pi} \frac{L}{r_C} \text{erf}\left(\frac{L}{2r_C}\right) \right)^2 f_{\text{corr}}, \end{aligned} \quad (14)$$

where f_{corr} describes the correlations, which, because of the particular geometry of LIGO and LISA Pathfinder, have the same form:

$$f_{\text{corr}} = \left[1 - e^{-\frac{L^2}{4r_C^2}} + \frac{1}{2} e^{-\frac{(a+L)^2}{4r_C^2}} \left(1 + e^{\frac{aL}{r_C^2}} - 2e^{\frac{L(2a+L)}{4r_C^2}} \right) \right]. \quad (15)$$

In the case of LIGO, an extra factor 2 appears in Eq. (14) to take into account the two arms of the interferometer. Since the measured spectral densities refer only to positive frequencies, one has to multiply the expressions in Eq. (11) and Eq. (14) by a factor 2 to take into account the conversion from the two-side to one-side spectra.

3. EXPERIMENTAL UPPER BOUNDS

3.1. Resonant detectors of gravitational waves: AURIGA

The first generation of gravitational wave detectors exploited simple and compact systems. The idea is to monitor the deformation of an elastic body, typically a massive ton-scale resonant bar or sphere, induced by a gravitational wave. The main drawback compared to interferometers, see below, is the smaller bandwidth and the shorter characteristic length ~ 1 m. However, as these detectors have been operated at cryogenic temperature and have achieved equally impressive displacement noise $\sqrt{S_{xx}} \sim 10^{-20} \text{ m Hz}^{-\frac{1}{2}}$, it is worth considering their sensitivity to CSL effects. As best case we consider AURIGA [24, 28], which is based on a aluminum (density of 2700 kg/m^3) cylinder with length $L = 3$ m, radius $R = 0.3$ m and mass $m = 2300$ kg cooled to $T = 4.2$ K, schematically represented in Fig. 1. Other detectors of the same class feature similar parameters.

The fundamental longitudinal mode at $\omega_0/2\pi \sim 900$ Hz is monitored by a sensitive SQUID-based readout [28]. This mode is equivalent to a reduced system of two masses $m/2$ connected by a spring and oscillating in counterphase with the same elongation of the bar extrema, so that the effective motional mass is comparable to that of the center of mass. For this reason, even if the mode does not actually represent center-of-mass motion, we will estimate the CSL effect using the CSL center-of-mass formula for the force noise spectrum, which has the analytical expression given by Eq. (11). We expect this procedure to yield a crude but reasonable estimate of the CSL effect, within a factor of 2. The equivalent force noise spectrum $S_{\text{FF}}(\omega)$ of the reduced system is related to the strain noise spectrum $S_{\text{hh}}(\omega)$

by the relation [24, 29]:

$$S_{\text{FF}}(\omega) = \left(\frac{m\omega_0^2 L}{\pi^2} \right)^2 S_{\text{hh}}(\omega), \quad (16)$$

from which we obtain the bounds on the CSL parameters. For the AURIGA detector in the current scientific run, the minimum strain noise at resonance is $S_{\text{h}}(\bar{\omega}) = \sqrt{S_{\text{hh}}(\bar{\omega})} = 1.6 \times 10^{-21} \text{ Hz}^{-1/2}$ at $\bar{\omega}/2\pi = 931 \text{ Hz}$ (in the following we will use single index to represent square rooted spectral densities). An independent absolute calibration was performed, based on the fluctuation-dissipation theorem, demonstrating that the noise at resonance is dominated by thermal noise [24]. The calibration accuracy was of the order of $\sim 10\%$ in energy. Taking this into account, we estimate the minimum unknown force noise, which could be attributed to CSL, as $S_{\text{F}} = 12 \text{ pN Hz}^{-1/2}$. Note that AURIGA (as well as NAUTILUS [31]) has been also operated in previous runs at lower temperatures $\sim 100 \text{ mK}$ [30]. The minimum strain noise at resonance was actually lower, but an accurate thermal noise calibration in that case was not performed. This results in a value for the minimum unknown force noise comparable to that given above.

The comparison of the CSL prediction with the experimental data leads to the red line and exclusion area in Fig. 2.

3.2. Interferometric detectors of gravitational waves: LIGO

Interferometric detectors of gravitational waves, such as LIGO [32] (as well as Virgo [33]), are essentially Michelson interferometers in which the two arms are configured as a Fabry-Perot cavities. A passing gravitational wave induces a differential change of the arm lengths, resulting in a phase change of the output light. Each arm includes two suspended test masses acting as end mirrors, placed at several km to each other (4 km for LIGO, 3 km for Virgo) to maximize the response to the gravitational wave strain h . The suspensions are made of actively controlled multistage pendulum systems, with resonant frequency $\omega_0/2\pi$ below 1 Hz, designed to heavily filter seismic noise. The last stage is designed for ultrahigh quality factor ($Q > 10^8$) in order to suppress as much as possible the thermal noise. The actual sensitivity band is roughly above $\sim 10 \text{ Hz}$, implying that the test masses can be considered to a good approximation in the free-mass limit $\omega \gg \omega_0$.

Interferometric detectors are typically characterized by the strain spectral density $S_{\text{hh}}(\omega)$, which is defined as the equivalent strain spectral density of an optimally oriented gravitational wave producing the observed noise at the output. Given the arm length a (see Fig. 1), the differential change $\Delta a = |\Delta a_x - \Delta a_y|$ of the two arm lengths induced by an optimally oriented strain h is predicted by General Relativity to be $\Delta a = ha$. It follows immediately that any displacement noise spectral density $S_{xx}^{\text{LIGO}}(\omega)$ of one of the two arms will cause an equivalent strain noise $S_{\text{hh}}^{\text{LIGO}}(\omega) = S_{xx}^{\text{LIGO}}(\omega)/a^2$. The former can be derived with the usual approach from Eqs. (12) by solving them in the frequency domain:

$$S_{xx}^{\text{LIGO}}(\omega) = \frac{4}{m^2} \frac{S_{\text{FF}}^{\text{LIGO}}(\omega)}{(\omega_0^2 - \omega^2)^2 + (\frac{\omega\omega_0}{Q})^2}, \quad (17)$$

where $S_{\text{FF}}^{\text{LIGO}}(\omega)$ is defined in Eq. (14). In this way, in the free-mass limit $\omega \gg \omega_0$, we can derive the expression for the equivalent strain induced by the CSL noise field.

From Eq. (17), we can argue that the CSL contribution to $S_{\text{hh}}(\omega)$ features a $1/\omega^4$ dependence, or a $1/\omega^2$ dependence when the square root spectrum $S_{\text{h}}(\omega)$ is considered. The minimum force noise and therefore the stronger upper bound on the CSL parameters will be achieved at a well-defined frequency $\bar{\omega}/2\pi$. As the typically measured $S_{\text{h}}(\omega)$ is convex [32], $\bar{\omega}/2\pi$ can be graphically inferred from the spectrum as the frequency at which $S_{\text{h}}(\omega)$, displayed in log-log scale, is tangent to a straight line with slope equal to -2 .

For Advanced LIGO at the time of the first detection [25, 34], $S_{\text{h}}(\bar{\omega})$ is in the range of $10^{-23} \text{ Hz}^{-1/2}$. From the published spectrum we infer that the effective force noise reaches a minimum $S_{\text{F}}(\bar{\omega}) \approx 95 \text{ fN Hz}^{-1/2}$ at $\bar{\omega}/2\pi \sim 30 - 35 \text{ Hz}$. We have used the numerical values $m = 40 \text{ kg}$ for the test mass and $a = 4 \text{ km}$ for the arm length. For the design sensitivity of Advanced LIGO, not yet reached, one can estimate from the design curves a minimum force $S_{\text{F}}(\bar{\omega}) \approx 25 \text{ fN Hz}^{-1/2}$ at $\bar{\omega}/2\pi \sim 15 - 20 \text{ Hz}$ [25, 32, 34]. Each test mass is a cylinder of fused silica (density of 2200 kg/m^3) with radius $R = 17 \text{ cm}$ and length $L = 20 \text{ cm}$.

By plugging the test mass parameters and the measured force noise in Eq. (14), we obtain the exclusion region for the CSL parameters shown in blue in Figure 2.

3.3. Space-based experiments: LISA Pathfinder

The last system we consider is LISA Pathfinder. This space mission has been recently launched as a technology demonstrator of the proposed space-based gravitational wave detector LISA. LISA concept is similar to terrestrial interferometric detectors, but will exploit a much longer baseline $\sim 10^6$ km and the more favourable conditions of operation in space. The detector will be sensitive to gravitational waves in the mHz range, thus providing different and complementary informations compared to ground-based detectors. LISA test masses will be in nearly ideal free-fall and essentially free from the vibrational, seismic and gravity gradient disturbances which unavoidably affect any terrestrial low-frequency experiment.

The main goal of LISA Pathfinder is to demonstrate the technology required by LISA, in particular to assess the accuracy of the achievable free-fall condition. The core of LISA Pathfinder consists in a pair of test masses in free-fall, protected by a satellite which follows the mass trying to minimize the stray disturbance, see Fig. 1. The overall objective is to demonstrate the performance required for test masses of LISA Pathfinder in terms of acceleration noise. Thus, the output of the experiment is directly expressed as a relative acceleration noise spectrum $S_{gg}(\omega)$, which is related to the relative force noise spectral density by the relation:

$$S_{gg}(\omega) = \frac{1}{m^2} S_{FF}(\omega). \quad (18)$$

The geometry of each test mass is straightforward: a cube of side $L = 4.6$ cm, made of an alloy of AuPt, with a mass of $m = 1.928$ kg, and the distance between the two masses equal to $a = 37.6$ cm. Thanks to the space operation, the force sensitivity is better than terrestrial experiments like LIGO. The current best experimental figure reaches a value of $S_{gg}(\omega) = 2.7 \times 10^{-29} \text{ m}^2 \text{ s}^{-4} \text{ Hz}$ [26].

To calculate the bound on CSL parameters, we consider directly $S_{FF}^{\text{LISA}}(\omega)$ as expressed in Eq. (14). By plugging the numerical values of the parameters and the best force noise, as given above, we obtain the green exclusion area in Figure 2.

4. DISCUSSION

The upper bounds on λ from the three experiments considered here have a very similar shape, achieving a minimum for r_C of the order of the test mass relevant length. For $r_C > 1$ m the three bounds are roughly comparable, with the one set by LIGO slightly better. Theoretically, such values of r_C are not much interesting, since already excluded by assuming the effective collapse of macroscopic objects [6] (gray region in Fig. 2). For short r_C , the best bound is set by LISA Pathfinder.

We observe that in general the bounds obtained here are the best so far for r_C ranging from roughly 1 μm up to the macroscopic scale, thereby excluding a substantial region of the parameter space. While this r_C interval is not the one usually considered relevant or theoretically favoured, we point out that, as long as r_C and λ are free parameters, unambiguous exclusion of a given parameter space can be done only through experiments. At the standard characteristic length $r_C = 10^{-7}$ m, the bound from LISA Pathfinder $\lambda < 3 \times 10^{-8}$ is still interesting, falling about a factor of 2 from the best limit obtained so far with mechanical techniques at ultralow temperature [23]. The strongest bound so far is still provided by X-ray experiments [22], although the latter requires stronger assumptions on the CSL noise spectrum.

We also note that the inferred bounds are conservative, at least for the LIGO and LISA Pathfinder cases, as we have assumed that all measured noise is attributed to CSL. Actually, the interferometer noise can be to a good extent characterized and attributed to well-defined sources. Subtraction of well-characterized noise may enable in principle a slight improvement of the bounds. For the AURIGA case, the noise at resonance is almost entirely due to thermal noise, and an absolute calibration based the fluctuation-dissipation theorem was performed. In this case a noise subtraction within the calibration uncertainty is entirely legitimate. For interferometers such as LIGO this task might be more difficult, as several noise sources combine together to yield the measured spectrum, depending on frequency. Some of them, such thermal noise, might be in principle fully characterized, but others, like newtonian or seismic noise, are definitely a worse case. For the LISA Pathfinder case, there is evidence that thermal noise from the residual gas is dominating the residual force noise. Unfortunately, uncertainties in the pressure, temperature and composition of the gas make it hard to perform an independent calibration based on the fluctuation-dissipation theorem [26].

We also mention that there is another class of macroscopic mechanical resonators, namely torsion balances, which have been the most sensitive force sensors since the time of Cavendish. We have not considered explicitly this class of experiments because typical sensor size ($10^{-2} - 1$ m) and frequency band (mHz) are very similar to the ones of

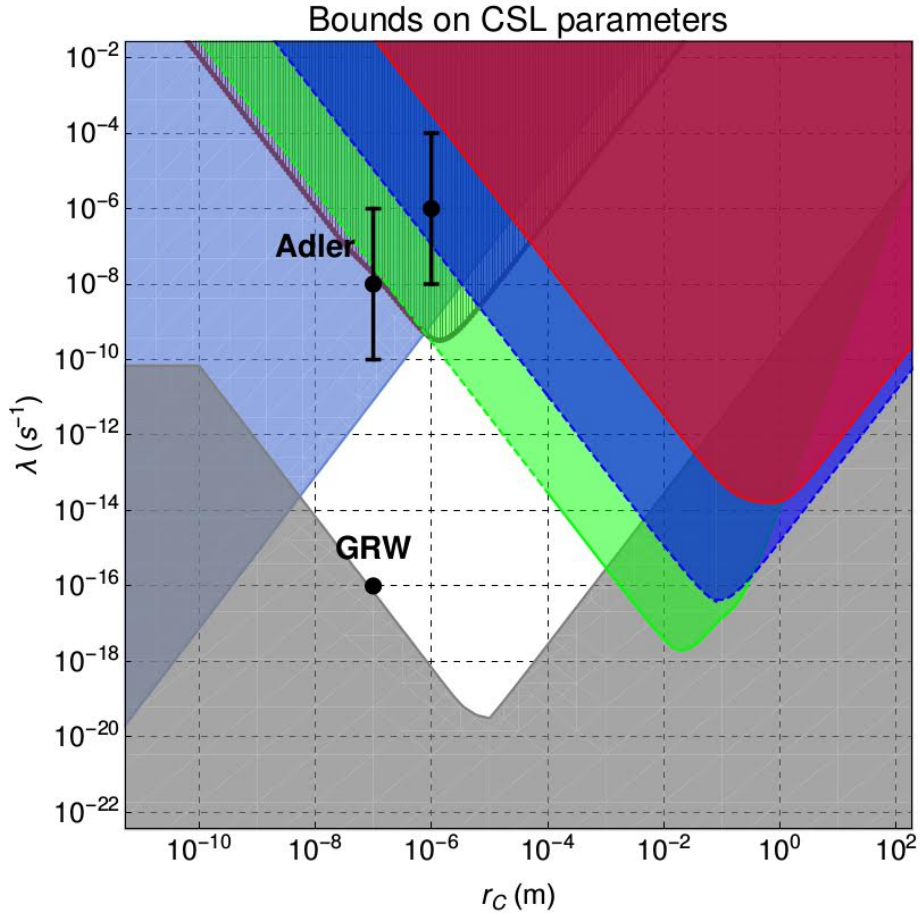


FIG. 2: Fig. 2. Upper and lower bounds on the CSL collapse rate λ as function of the characteristic length r_C . Red, blue and green lines (and respective shaded regions): upper bounds (and exclusion regions) on the CSL model from the AURIGA, LIGO and LISA Pathfinder experiments. Purple line: upper bound from ultracold cantilever experiments [23]. Light blue line: Best upper bound from X-ray experiments [22]. Gray line: lower bound on CSL model based on theoretical arguments [6]. The GRW [1] and Adler [5] values and ranges are indicated by black dots.

LISA Pathfinder. In fact, ground testing of LISA technology has been done primarily by means of torsion pendulum experiments. However, the actual performances achieved by LISA Pathfinder have arguably improved over ground-based tests by at least 2 orders of magnitude [26].

Finally, we discuss future prospects. For the present class of interferometers like Advanced LIGO or Advanced Virgo, a significant improvement is expected in the next 2-3 years, with these detectors likely approaching the design sensitivity. The bound would not be as good as LISA Pathfinder at short r_C , but it would further extend the exclusion region at $r_C > 1$ m. The third generation of interferometers, currently under study, will employ cryogenic suspensions for a further reduction of low frequency noise by 1-2 orders of magnitude. This will enable an improvement of the CSL bounds over LISA Pathfinder. Inversely, we note that if a CSL noise will eventually appear in the range of parameters predicted by Adler, this would limit the low-frequency sensitivity of future generation of interferometers. While this scenario might seem unlikely, it seems it was never clearly pointed out.

On the other hand, strong improvements are expected by space missions in the near and far future. LISA Pathfinder is still under operation and the noise is slowly but steadily improving with time. This suggests that the dominating noise contribution is thermal noise from residual gas, with slowly decreasing pressure. Within the next 12 months the noise may further improve and strengthen the bounds. On the other hand, LISA Pathfinder has essentially reached the requirements for the future LISA mission in terms of residual acceleration noise. While no substantial improvement is required by LISA, it is reasonable to expect further significant improvements in the next decade before the launch. Other missions under study, such as MAQRO, will try to exploit the beneficial aspects of space environment in interferometric or force-sensing experiments with nanoparticles with size around 10^{-7} m [35]. This may open the way to a full test of CSL and other collapse models in a more relevant range of parameters.

Note. Preliminary results presented at 115th Statistical Mechanics Conference, Rutgers University 8-10 May 2016, and at the Quantum Control of Levitated Optomechanics COnference, Pontremoli, 18-20 May 2016. During the completion of this paper, we became aware of a related work by B. Helou *et al.*, deriving upper limits on collapse models from LISA Pathfinder data.

ACKNOWLEDGEMENTS

MC and AB acknowledge support from the University of Trieste and INFN. AV thanks S. Vitale and K. Danzmann for discussions on LISA Pathfinder and on the relevance of collapse models for the LISA Pathfinder mission.

* Electronic address: matteo.carlesso@ts.infn.it

† Electronic address: bassi@ts.infn.it

- [1] G.C. Ghirardi, A. Rimini, and T. Weber, Phys. Rev. D **34**, 470 (1986).
- [2] A. Bassi, and G.C. Ghirardi, Phys. Rep. **379**, 257 (2003).
- [3] A. Bassi, K. Lochan, S. Satin, T. P. Singh, and H. Ulbricht, Rev. Mod. Phys. **85**, 471 (2013).
- [4] G.C. Ghirardi, P. Pearle, and A. Rimini, Phys. Rev. A **42**, 78 (1990); G. C. Ghirardi, R. Grassi, and F. Benatti, Found. Phys. **25**, 5 (1995).
- [5] S.L. Adler, J. Phys. A **40**, 2935 (2007).
- [6] M. Toroš and A. Bassi, arXiv 1601.03672 (2016).
- [7] K. Hornberger, S. Gerlich, P. Haslinger, S. Nimmrichter and M. Arndt, Rev. Mod. Phys. **84**, 157 (2012).
- [8] T. Juffmann, H. Ulbricht and M. Arndt, Rep. Prog. Phys. **76**, 086402 (2013).
- [9] M. Arndt and K. Hornberger, Nat. Phys. **10**, 271 (2014).
- [10] M. Toroš and A. Bassi, arXiv 1601.03672 (2016).
- [11] W. Marshall, C. Simon, R. Penrose, and D. Bouwmeester, Phys. Rev. Lett. **91**, 130401 (2003).
- [12] J. van Wezel, T.H. Oosterkamp, Proc. R. Soc. A **468**, 35 (2012).
- [13] O. Romero-Isart, Phys. Rev. A **84**, 052121 (2011).
- [14] B. Collett and P. Pearle, Found. Phys. **33**, 1495 (2003).
- [15] S.L. Adler, J. Phys. A **38**, 2729 (2005).
- [16] M. Bahrani, M. Paternostro, A. Bassi, and H. Ulbricht, Phys. Rev. Lett. **112**, 210404 (2014).
- [17] S. Belli et al., arXiv 1601.07927 (2016).
- [18] S. Nimmrichter, K. Hornberger, and K. Hammerer, Phys. Rev. Lett. **113**, 020405 (2014).
- [19] L. Diosi, Phys. Rev. Lett. **114**, 050403 (2015).
- [20] D. Goldwater, M. Paternostro, P.F. Barker, arXiv:1506.08782 (2015).
- [21] J. Li, S. Zippilli, J. Zhang, D. Vitali, arXiv:1508.00466 (2015).
- [22] C. Curceanu, B. C. Hiesmayr, and K. Piscicchia, J. Adv. Phys. **4**, 263 (2015).
- [23] A. Vinante, M. Bahrani, A. Bassi, O. Usenko, G. Wijts, T.H. Oosterkamp, Phys. Rev. Lett. **116**, (2016).
- [24] A. Vinante (for the AURIGA Collaboration), Class. Quantum Grav. **23**, S103 (2006).
- [25] B.P. Abbott et al., Phys. Rev. Lett. **116**, 131103 (2016).
- [26] M. Armano et al, Phys. Rev. Lett. **116**, 231101 (2016).
- [27] S.L. Adler et al., J. Phys. A, **46**, 24 (2013).
- [28] L. Baggio et al., Phys. Rev. Lett. **94**, 241101 (2005).
- [29] M. McHugh et al., Class. Quantum Grav. **22**, S965 (2005).
- [30] J.P. Zendri et al. in "Gravitational waves", Proceedings of the "Third Edoardo Amaldi Conference", (CalTech - California, 1999), edited by S.Meshkov, AIP Conference Proceedings, New York (2000) p. 421-422.
- [31] P. Astone et al., Astropart. Phys. **7**, 231 (1997).
- [32] The LIGO Scientific Collaboration, Class. Quantum Grav. **32**, 074001 (2015).
- [33] F. Acernese et al., Class. and Quantum Grav. **32**, 024001 (2015).
- [34] B.P. Abbott et al., Phys. Rev. Lett. **116**, 061102 (2016).
- [35] R. Kaltenbaek et al., Exp. Astron. **34**, 123-164 (2012).